Controllable Photonic Time-Bin Qubits from a Quantum Dot

J. P. Lee,[1,2,*] L. M. Wells,[1,3] B. Villa,[1,3] S. Kalliakos,[1] R. M. Stevenson,[1] D. J. P. Ellis,[1]
I. Farrer,[3,†] D. A. Ritchie,[3] A. J. Bennett,[1,‡] and A. J. Shields[1]

[1]*Toshiba Research Europe Limited, Cambridge Research Laboratory,
208 Science Park, Milton Road, Cambridge, CB4 0GZ, United Kingdom*
[2]*Engineering Department, University of Cambridge, 9 J. J. Thomson Avenue,
Cambridge CB3 0FA, United Kingdom*
[3]*Cavendish Laboratory, Cambridge University, J. J. Thomson Avenue,
Cambridge CB3 0HE, United Kingdom*

Photonic time-bin qubits are well suited to transmission via optical fibers and waveguide circuits. The states take the form $\frac{1}{\sqrt{(2)}}(\alpha|0\rangle + e^{i\phi}\beta|1\rangle)$, with $|0\rangle$ and $|1\rangle$ referring to the early and late time bin, respectively. By controlling the phase of a laser driving a spin-flip Raman transition in a single-hole-charged InAs quantum dot, we demonstrate complete control over the phase, ϕ. We show that this photon generation process can be performed deterministically, with only a moderate loss in coherence. Finally, we encode different qubits in different energies of the Raman scattered light, paving the way for wavelength-division multiplexing at the single-photon level.

DOI: 10.1103/PhysRevX.8.021078   Subject Areas: Photonics, Quantum Information

I. INTRODUCTION

Quantum dots (QDs) have unparalleled brightness as single-photon sources and can be embedded in a variety of semiconductor devices and microcavity structures [1,2]. Until recently, the qualities of the photons generated from quantum dots have lagged behind other sources such as trapped atoms and ions, which enable the creation of photons with high indistinguishabilities and controllable temporal profiles via stimulated Raman transitions [3–5]. These Raman techniques have also been shown to enable the control of the polarization of the emitted photons by setting the laser parameters [6], the heralding of entanglement between distant solid-state spins [7], and the creation of solid-state, single-photon sources in integrated nanophotonic circuits [8].

However, in the past few years, researchers have demonstrated almost perfectly indistinguishable photons from a

---

*james.patrick.lee.47@gmail.com

†Present address: Department of Electronic & Electrical Engineering, University of Sheffield, Mappin Street, Sheffield S1 3JD, United Kingdom.

‡Present address: Institute for Compound Semiconductors, Cardiff University, Queen's Buildings, 5 The Parade, Roath, Cardiff CF24 3AA, United Kingdom.

resonantly excited QD [9], control over the spectrum of resonantly scattered light [10,11], and the filtering of the phonon sideband and improvement of photon coherence through the use of micropillar cavities [12,13].

Inspired by atomic physics, the use of Raman scattering in quantum dots has been used to demonstrate photon energy tuning [14], generation of photons tailored for interfacing with a quantum memory [15], picosecond shaping of single photons [16], and generation of photons coherently superposed across multiple time bins [17].

In this work, we use cavity-enhanced Raman scattering to generate a single-photon, time-bin-encoded qubit superposed across two time bins. We show that modulating the phase difference between the driving laser pulses results in the modulation of the phase difference between the time bins of the generated single-photon state, enabling complete control of a time-bin qubit without the use of an interferometer. Next, we show that the coherence between the two time bins remains when the Raman transition is driven deterministically at higher laser powers. Finally, we use two driving lasers detuned to either side of the Raman transition; we encode a different time-bin qubit with each laser and show that spectral filtering enables us to recover the encoded state for each frequency.

II. SETUP

Our experimental setup is illustrated in Fig. 1(a). We use a single-hole-charged InAs QD held in a Voigt geometry magnetic field, which results in a double-lambda system, as illustrated in Fig. 1(c). A narrow linewidth laser (or two
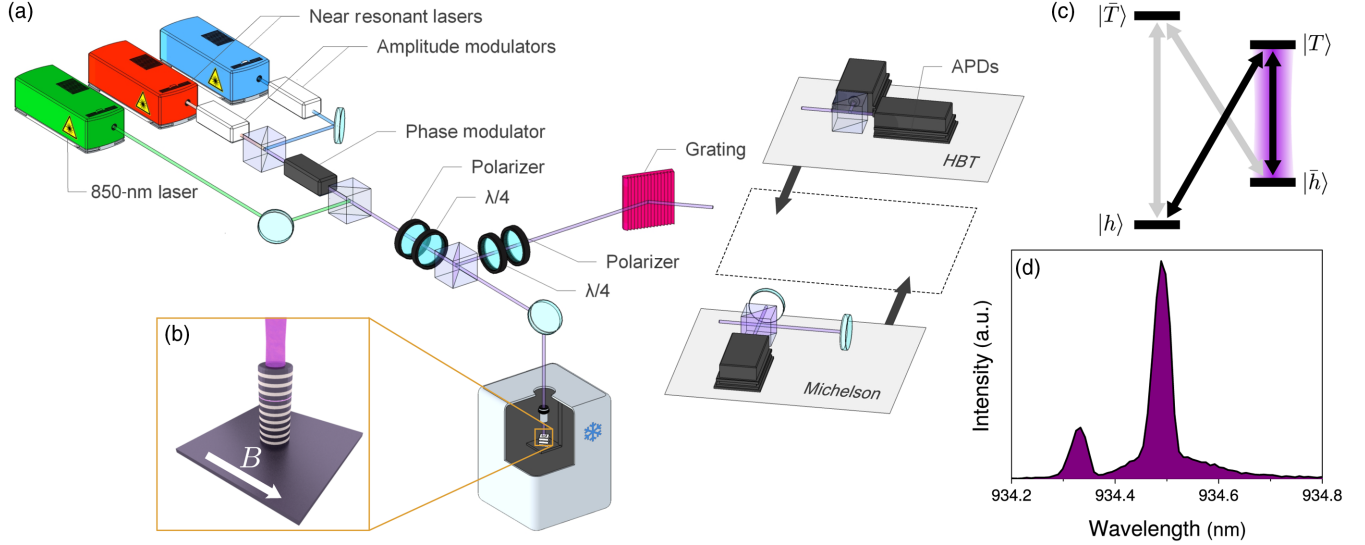
FIG. 1.   (a) An illustration of our experimental setup. (b) An illustration of a micropillar cavity in a Voigt geometry magnetic field. (c) The energy-level diagram. When the resonant lasers are red or blue detuned from the diagonal transition, the resulting Raman scattered light is similarly detuned. (d) The spectrum of the QD under nonresonant excitation. Polarization filtering ensures that only the vertical transitions are visible, and the long-wavelength transition is clearly enhanced by the cavity mode.

narrow linewidth lasers for the wavelength control experiment) is used to drive the diagonal $|h\rangle \rightarrow |T\rangle$ transition, where $|h\rangle$ and $|\bar{h}\rangle$ ($|T\rangle$ and $|\bar{T}\rangle$) represent orthogonal hole (positive trion) states. Amplitude and phase modulators are used to control the excitation laser light. A micropillar cavity [Fig. 1(b)] is used to increase the collection efficiency and to selectively Purcell enhance emission from the longest wavelength transition. In addition to the Raman scattered light having a longer wavelength than the input light, it is also orthogonally polarized [18], which allows us to use polarization and spectral filtering to separate the driving laser light from the emitted light. Our sample is nominally undoped, so we use a pulsed nonresonant laser to generate charge carriers in the sample in order to introduce a hole spin [12,19]. The spectrum under nonresonant excitation is shown in Fig. 1(d).

III. ARBITRARY TIME-BIN QUBITS

A. Phase modulation

Once we have injected a hole into the dot with a nonresonant laser pulse, we use two resonant pulses that drive the diagonal transition to create a photon superposed across two time bins. The second resonant pulse requires a higher intensity than the first to compensate for the depletion of the $|h\rangle$ state caused by the first resonant pulse. The outcome is that the photon is equally likely to be measured in each time bin. The capability to produce photons superposed across time bins in this manner has been demonstrated in Ref. [17], but here we demonstrate control over the phase difference between the time bins. In principle, this could be done by placing a phase modulator

at the output [20], but this introduces losses (at wavelengths of about 940 nm, the loss is typically around 3 dB). In our experiments, we show that we can achieve the same result without the associated losses by phase modulating the input resonant driving laser and increasing the laser intensity to account for the loss.

The pulse sequence used is shown in Fig. 2(a). A hole is introduced by a nonresonant pulse of about 50 ps. Then, a non-phase-modulated, two-pulse sequence that is resonant with the diagonal $|h\rangle \rightarrow |T\rangle$ transition is used to create a photon with the energy of the $|T\rangle \rightarrow |\bar{h}\rangle$ transition. Each resonant pulse is about 400 ps in duration, with a pulse separation of 1.5 ns.

Assuming that the system begins in the $|h\rangle$ state due to the nonresonant pulse, the pulse sequence works as follows:

(1) The resonant pulse at τ_1 drives the Raman transition with probability p_1, resulting in the state $\sqrt{1-p_1}|h\rangle|0_{\tau_1}\rangle + \sqrt{p_1}|\bar{h}\rangle|1_{\tau_1}\rangle$, where $|0\rangle$ ($|1\rangle$) represents the absence (presence) of a photon in a time bin.

(2) The second resonant pulse drives the Raman transition with a probability p_2, resulting in the state $\sqrt{1-p_1}\sqrt{1-p_2}|h\rangle|0_{\tau_1}\rangle|0_{\tau_2}\rangle + \sqrt{p_1}|\bar{h}\rangle|1_{\tau_1}\rangle|0_{\tau_2}\rangle + \sqrt{1-p_1}\sqrt{p_2}|\bar{h}\rangle|0_{\tau_1}\rangle|1_{\tau_2}\rangle$. In order to obtain an equal probability of having a photon in each time bin, we require that the second and third terms of this state have equal coefficients, i.e., $\sqrt{p_1} = \sqrt{1-p_1}\sqrt{p_2}$. This means that, in general, we require the second excitation pulse to be brighter than the first. In the fully deterministic case, where a photon is generated with unit probability, we have that $p_1 = \frac{1}{2}$ and $p_2 = 1$.
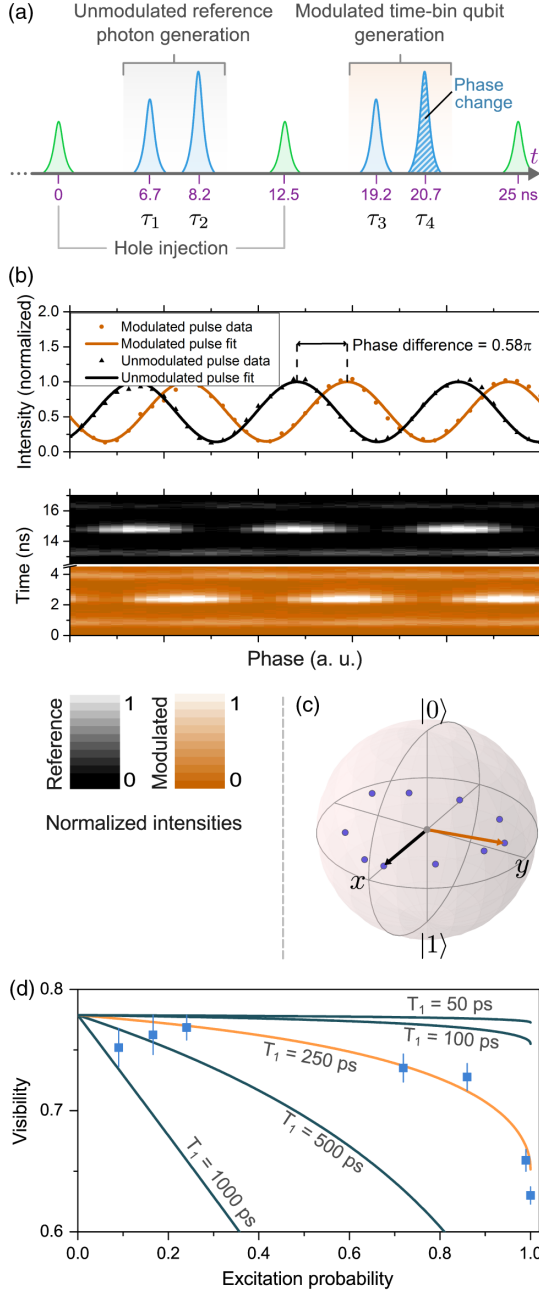
FIG. 2. (a) An illustration of the pulse sequence used to demonstrate phase control over a time-bin qubit. (b) The extracted interference fringes for reference (black) and phase modulated (orange) photons. We show the time-resolved plots of the interference between neighboring time bins for the two sequences that allow us to extract the interference fringes and the probabilities of measuring the photon in each time bin. (c) The recorded time-bin qubits mapped onto the Bloch sphere (blue points). The black and orange vectors represent the states generated by reference and example modulated pulse sequences, respectively. (d) The measured interference visibility as a function of photon generation probability (blue data points) and the calculated expected interference visibility for several different radiative decay times (lines).

(3) The measurement of a photon then projects the hole into the $|\bar{h}\rangle$ state, leaving us with the state $\frac{1}{\sqrt{(2)}}|\bar{h}\rangle(|1_{\tau_1}\rangle|0_{\tau_2}\rangle + |0_{\tau_1}\rangle|1_{\tau_2}\rangle)$, assuming that $\sqrt{p_1} = \sqrt{1-p_1}\sqrt{p_2}$. Factoring out the hole state, we get the time-bin-encoded photonic state: $\frac{1}{\sqrt{(2)}}(|1_{\tau_1}\rangle|0_{\tau_2}\rangle + |0_{\tau_1}\rangle|1_{\tau_2}\rangle)$.

The photons generated by the pulses at τ_1 and τ_2 serve as a reference for photons generated by the second set of excitation pulses at τ_3 and τ_4.

Then, the hole state is randomized by a second nonresonant pulse to ensure that there is some nonzero probability that the hole is in the $|h\rangle$ state (as in Ref. [17]) in order to allow the generation of a second photon. The resonant pulses at τ_3 and τ_4 are used to create a second photon superposed between time bins, but this time, the phase modulator is used to modify the phase of the fourth resonant pulse. The entire six-pulse sequence is repeated at a frequency of 40 MHz. Directing the light through an unbalanced Michelson interferometer to observe interference between the early and late time bins and time resolving the output, we can determine the phase difference between the time bins. The photons generated by the pulses at τ_1 and τ_2 serve as a reference for the interference measurement with no phase modulation, allowing us to extract the phase difference due to the modulator.

Figure 2(b) shows the result of the experiment for a phase modulation of 0.58π. The phase change due to the phase modulator is determined by calculating the phase difference between the interference fringes created using the unmodulated reference sequence and modulated sequence [Fig. 2(b)]. The phase modulation has no apparent effect on the interference visibility, with the mean recorded interference visibility being $73.7 \pm 1.1\%$. The factors limiting this visibility will be discussed in Sec. III B.

Taking the phase difference of $\phi = 0$ to represent the $|+\rangle = \frac{1}{\sqrt{(2)}}(|0\rangle + |1\rangle)$ state, using the intensity recorded in the early and late time bins to extract the amplitudes of the $|0\rangle$ and $|1\rangle$ components of the state, and using the interference visibility to help determine the magnitudes of the off-diagonal elements of the density matrix, we plot the generated states on the Bloch sphere. We determine that we can achieve phase shifts of up to 2.94π [only shifts below 2π are shown in Fig. 2(c)]. This shows that we can freely control the phase ϕ of the time-bin qubit. It is trivial to change the amplitude of the $|0\rangle$ and $|1\rangle$ states by controlling the intensity of the resonant laser pulses, allowing us to conclude that we can use this method to generate any qubit state.

This modulation technique could be expanded to higher-dimensional states such as those demonstrated in Ref. [17] in order to create arbitrary time-bin-encoded qudits.

High-dimensional single-photon qudits can be used in quantum communication protocols [21–24] and are of interest for quantum computing applications; the use of high-dimensional states means that the dimensionality of the Hilbert space needed to describe the states grows faster with photon number than for two-dimensional qubit states [25].

B. Coherence and deterministic excitation

The output photons can be generated in one of two ways: They can be generated coherently by the Raman spin-flip process or by the excitation of the diagonal transition from the resonant laser and the subsequent incoherent decay. In Refs. [14,26], the authors note that the two processes can be distinguished by their linewidths—the linewidth of the Raman scattered photons is determined by the laser linewidth and the trapped spin coherence time, whereas the linewidth of the photons resulting from the incoherent decay is typically broader and has the linewidth of the cavity-enhanced optical transition. The authors of Ref. [14] observe that, in part due to the cavity enhancement, the Raman process dominates.

In analogy with resonant Rayleigh scattering, we investigate whether the power of the driving laser increases the proportion of incoherently scattered light [12]. Using a two-level model as in Ref. [26], we expect the ratio between the coherently scattered and incoherently scattered light to be [27]

$$\frac{I_{\text{coherent}}}{I_{\text{total}}} = \frac{2\Gamma^2}{2\Gamma^2 + \Omega^2}, \tag{1}$$

where $\Gamma = 1/T_1$ is the radiative decay rate (T_1 is the radiative decay time) and Ω is the Rabi frequency.

In our work, we only expect to see interference between the time bins when the photons are produced by Raman scattering. This means that we expect to see a reduction in the interference visibility as the incoherent fraction increases with increasing Rabi frequency.

In order to investigate this effect experimentally, we set the ratio between the first and second resonant laser pulses to be 1∶4 in intensity. As the angle of the rotation about the Bloch sphere for a given pulse is proportional to the square root of the power, this means that the second pulse rotates the Bloch vector by twice the angle of the first pulse. We then adjust the laser power such that the measured intensity of the output light was equal in each time bin and conclude that this means we are driving the $|h\rangle$ to $|T\rangle$ transition with a $\pi/2$ and a π pulse for the first and second laser pulses, respectively (this ensures that $\sqrt{p_1} = \sqrt{1 - p_1}\sqrt{p_2}$). Therefore, provided the system is in the $|h\rangle$ state initially, this process deterministically creates a photon. Given that this process is limited to a maximum of a single photon per cycle of the pulse sequence (or until a spontaneous spin flip occurs—this is typically on the scale of microseconds

[28], several orders of magnitude longer than the pulse sequence), it does not make sense to consider higher powers than this. We perform the interference measurement at this power and at several lower powers—we have plotted the resulting interference visibilities in Fig. 2(d). We observe that the interference visibility decreases at high laser driving powers, but the Raman process still dominates.

Using Eq. (1), we can plot out the expected interference visibility as a function of the probability of generating a photon. The maximum achievable visibility is determined by the coherence time of the trapped spin. Estimating a coherence time of about 6 ns gives reasonable agreement with our results (resulting in a maximum possible visibility of 77.8% when accounting for the 1.5-ns pulse separation time) and is within the range of previously measured values for the coherence time of a trapped hole spin [26,29,30]. In future implementations of this scheme, the use of dynamical decoupling and nuclear field quietening techniques could extend the coherence time of the trapped hole spin [31,32]—a spin coherence time of 1 μs would increase the maximum possible visibility to 99.85%.

We then assume that any reduction in the interference visibility below 77.8% is due to the reduction of the coherent fraction of the scattered light. We use the Rabi frequency of the second (the brightest) pulse to calculate the expected resulting interference visibility as a function of the probability of generating a photon. We plot the expected visibilities for several different values of T_1 and see that $T_1 = 250$ ps gives good agreement with our experimental results.

We note that for shorter T_1 times, the coherence degrades less with photon generation probability. We anticipate that using higher Purcell factor systems to reduce the radiative decay time would increase the coherent fraction and thus increase the interference visibility. It may also be possible to increase the coherent fraction by detuning the cavity and the resonant laser from the $|T\rangle \rightarrow |\bar{h}\rangle$ transition line, as in Ref. [14]. Moving beyond the simple two-level model in this way may enable the cavity enhancement of the coherent Raman scattered light without directly enhancing the transition.

Our current setup has a relatively small Purcell factor; nevertheless, the Raman process dominates at all photon-generation probabilities, indicating that this spin-flip Raman scattering technique holds promise for the deterministic generation of arbitrary, d-dimensional, single-photon qudits.

IV. WAVELENGTH CONTROL

We now demonstrate the wavelength control of a single-photon source. Encoding information in different degrees of freedom of single photons is a topic of current interest for quantum communication [33].

The tuning of the energy of the Raman scattered photons by tuning the driving laser energy has been demonstrated [14]. The ability to tune the photon energy is considered
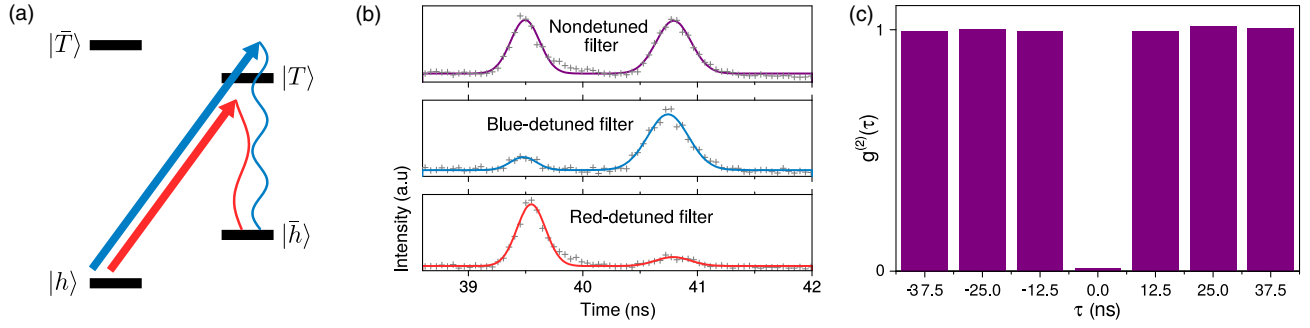
FIG. 3.   (a) An illustration of driving the Raman transition with a red- and a blue-detuned laser. (b) A time-resolved plot and fit of the output light when a red-detuned laser is used to drive the Raman transition in time bin 1 and a blue-detuned laser is used to drive the transition in time bin 2, shown for the following situations: The spectral filter is not detuned (top panel); the spectral filter is blue detuned (middle panel); the spectral filter is red detuned (bottom panel). (c) The result of a second-order correlation function measurement on the Raman scattered light generated using two detuned lasers, both of which are pulsed in time bins 1 and 2.

important as it enables photons from different sources to be made indistinguishable and thus suitable for many quantum communication and computing applications. Here, we use the tunability of Raman scattered photons to encode a different photonic state at two different energies. We use two lasers, red and blue detuned from the diagonal transition by about 10 μeV, resulting in a total energy separation of 19.1 μeV [illustrated in Fig. 3(a)].

In general, a wavelength-division-multiplexed time-bin-encoded state generated by this process will have the form

$$|\psi\rangle = \gamma|\text{red}\rangle(\alpha_r|0\rangle + e^{i\phi_r}\beta_r|1\rangle)$$
$$+ e^{i\phi}\delta|\text{blue}\rangle(\alpha_b|0\rangle + e^{i\phi_b}\beta_b|1\rangle), \quad (2)$$

where $|\text{red}\rangle$ ($|\text{blue}\rangle$) indicates the state generated by the red-(blue-) detuned laser.

In our experiment, we apply a pulse in time bin 1 with the red-detuned laser, encoding the $|0\rangle$ state, and we apply a pulse in time bin 2 with the blue-detuned laser, encoding the $|1\rangle$ state. The output state should therefore be

$$|\psi\rangle = \frac{1}{\sqrt{2}}(|\text{red}\rangle|0\rangle + e^{i\phi}|\text{blue}\rangle|1\rangle). \quad (3)$$

Measuring the output shows a roughly equal probability of measuring the $|0\rangle$ or the $|1\rangle$ state [Fig. 3(b)]. However, spectrally filtering the output using a diffraction grating enables us to recover the $|0\rangle$ state for red detuning and the $|1\rangle$ state for blue detuning [Fig. 3(b)], with probabilities of 0.81 and 0.86, respectively.

As the lasers have no set phase relationship with one another (i.e., we expect the phase ϕ to be random), we do not expect to see interference between the two time bins. In this case, we cannot confirm that this is a coherent superposition state. Future work could create the desired excitation spectrum by modulating and filtering light from a single laser or by phase locking the two driving lasers in order to investigate the possibility of producing coherent

superpositions of frequencies for single photons. This would enable the creation of states like the one shown in Eq. (2), enabling single-photon wavelength-division multiplexing.

Finally, we demonstrate that this process does indeed generate single photons by performing a second-order correlation function measurement [Fig. 3(c)]. We use time tagging to remove any influence from photons generated by the nonresonant pulse and consider only the photons generated by the resonant laser pulses. This measurement is performed on light generated using both detuned lasers, with both lasers being modulated so that there are two pulses at each wavelength. The filtering is set so that both red- and blue-detuned photons can trigger both detectors. We obtain a value of $g^{(2)}(0) = 0.01$, indicating that the output light is primarily composed of single photons, as expected due to the timescale of spontaneous spin flips being orders of magnitude longer than the pulse separation. We attribute the nonzero $g^{(2)}(0)$ to leakage of the resonant laser into the detection setup.

V. CONCLUSIONS

We have demonstrated that we can produce arbitrary single-photon time-bin-encoded qubits and that we can, in principle, do so deterministically, albeit with some loss in coherence. We then demonstrated that this cavity-stimulated Raman process can be used to control the wavelength of the generated photons. We anticipate that this will enable single-photon wavelength-division multiplexing when lasers with a controlled phase relationship are used. In combination with prior work, these results demonstrate the capability to encode large amounts of information with a single photon using the photon energy and high-dimensional, arbitrary time-bin-encoded states.

VI. METHODS

We make use of a QD cavity system that is cooled to 5 K and placed in a 5.5-T Voigt geometry magnetic field.

The micropillar cavity is 2.5 μm in diameter and has a quality factor of about 5000. We estimate that the Purcell factor for the long wavelength transition is about 4 by comparing the intensity of the enhanced and nonenhanced transitions. Our pulsed nonresonant laser generates light at a wavelength of 850 nm, and our resonant laser was set to a wavelength of 934.18 nm. The amplitude modulation was performed using fiber-coupled LiNbO$_3$ electro-optic amplitude modulators. The phase is controlled with a LiNbO$_3$ electro-optic phase modulator designed for wavelengths of 1.3 μm; at 940 nm, the transmission is about 40%. The output light is measured with silicon APDs with an efficiency of 30%—the typical count rate observed due to the Raman scattered light is in the range of 10–50 kHz.

VII. DATA ACCESS

The experimental data used to produce the figures in this paper are publicly available at [34].

ACKNOWLEDGMENTS

[1] S. Maier, P. Gold, A. Forchel, N. Gregersen, J. Mørk, S. Höfling, C. Schneider, and M. Kamp, *Bright Single Photon Source Based on Self-Aligned Quantum Dot-Cavity Systems*, Opt. Express **22**, 8136 (2014).

[2] M. Pelton, C. Santori, J. Vucković, B. Zhang, G. S. Solomon, J. Plant, and Y. Yamamoto, *Efficient Source of Single Photons: A Single Quantum Dot in a Micropost Microcavity*, Phys. Rev. Lett. **89**, 233602 (2002).

[3] A. Kuhn, M. Hennrich, and G. Rempe, *Deterministic Single-Photon Source for Distributed Quantum Networking*, Phys. Rev. Lett. **89**, 067901 (2002).

[4] J. Beugnon, M. P. A. Jones, J. Dingjan, B. Darquié, G. Messin, A. Browaeys, and P. Grangier, *Quantum Interference between Two Single Photons Emitted by Independently Trapped Atoms*, Nature (London) **440**, 779 (2006).

[5] G. S. Vasilev, D. Ljunggren, and A. Kuhn, *Single Photons Made-to-Measure*, New J. Phys. **12**, 063024 (2010).

[6] C. Kurz, J. Huwer, M. Schug, P. Müller, and J. Eschner, *A High-Rate Source for Single Photons in a Pure Quantum State*, New J. Phys. **15**, 055005 (2013).

[7] H. Bernien, B. Hensen, W. Pfaff, G. Koolstra, M. S. Blok, L. Robledo, T. H. Taminiau, M. Markham, D. J. Twitchen, L. Childress *et al.*, *Heralded Entanglement between Solid-State Qubits Separated by Three Metres*, Nature (London) **497**, 86 (2013).

[8] A. Sipahigil, R. E. Evans, D. D. Sukachev, M. J. Burek, J. Borregaard, M. K. Bhaskar, C. T. Nguyen, J. L. Pacheco, H. A. Atikian, C. Meuwly *et al.*, *An Integrated Diamond Nanophotonics Platform for Quantum Optical Networks*, Science **354**, 847 (2016).

[9] Y.-M. He, Y. He, Y.-J. Wei, D. Wu, M. Atatüre, C. Schneider, S. Höfling, M. Kamp, C.-Y. Lu, and J.-W. Pan, *On-Demand Semiconductor Single-Photon Source with Near-Unity Indistinguishability*, Nat. Nanotechnol. **8**, 213 (2013).

[10] C. Matthiesen, A. N. Vamivakas, and M. Atatüre, *Subnatural Linewidth Single Photons from a Quantum Dot*, Phys. Rev. Lett. **108**, 093602 (2012).

[11] C. Matthiesen, M. Geller, C. H. H. Schulte, C. Le Gall, J. Hansom, Z. Li, M. Hugues, E. Clarke, and M. Atatüre, *Phase-Locked Indistinguishable Photons with Synthesized Waveforms from a Solid-State Source*, Nat. Commun. **4**, 1600 (2013).

[12] A. J. Bennett, J. P. Lee, D. J. P. Ellis, T. Meany, E. Murray, F. F. Floether, J. P. Griffths, I. Farrer, D. A. Ritchie, and A. J. Shields, *Cavity-Enhanced Coherent Light Scattering from a Quantum Dot*, Sci. Adv. **2**, e1501256 (2016).

[13] P. Senellart, G. Solomon, and A. White, *High-Performance Semiconductor Quantum-Dot Single-Photon Sources*, Nat. Nanotechnol. **12**, 1026 (2017).

[14] T. M. Sweeney, S. G. Carter, A. S. Bracker, M. Kim, C. S. Kim, L. Yang, P. M. Vora, P. G. Brereton, E. R. Cleveland, and D. Gammon, *Cavity-Stimulated Raman Emission from a Single Quantum Dot Spin*, Nat. Photonics **8**, 442 (2014).

[15] L. Béguin, J.-P. Jahn, J. Wolters, M. Reindl, R. Trotta, A. Rastelli, F. Ding, Y. Huo, O. G. Schmidt, P. Treutlein *et al.*, *On-Demand Semiconductor Source of 780 nm Single Photons with Controlled Temporal Wave Packets*, Phys. Rev. X **97**, 205304 (2018).

[16] B. C. Pursley, S. G. Carter, M. K. Yakes, A. S. Bracker, and D. Gammon, *Picosecond Pulse Shaping of Single Photons Using Quantum Dots*, Nat. Commun. **9**, 115 (2018).

[17] J. Lee, A. Bennett, R. M. Stevenson, D. J. P. Ellis, I. Farrer, D. A. Ritchie, and A. J. Shields, *Multi-Dimensional Photonic States from a Quantum Dot*, Quantum Sci. Technol. **3**, 024008 (2018).

[18] R. J. Warburton, *Single Spins in Self-Assembled Quantum Dots*, Nat. Mater. **12**, 483 (2013).

[19] A. J. Bennett, J. P. Lee, D. J. P. Ellis, I. Farrer, D. A. Ritchie, and A. J. Shields, *A Semiconductor Photon-Sorter*, Nat. Nanotechnol. **11**, 857 (2016).

[20] H. P. Specht, J. Bochmann, M. Mücke, B. Weber, E. Figueroa, D. L. Moehring, and G. Rempe, *Phase Shaping of Single-Photon Wave Packets*, Nat. Photonics **3**, 469 (2009).

[21] H. Bechmann-Pasquinucci and W. Tittel, *Quantum Cryptography Using Larger Alphabets*, Phys. Rev. A **61**, 062308 (2000).

[22] T. Zhong, H. Zhou, R. D. Horansky, C. Lee, V. B. Verma, A. E. Lita, A. Restelli, J. C. Bienfang, R. P. Mirin, T. Gerrits, S. W. Nam, F. Marsili, M. D. Shaw, Z. Zhang, L. Wang,

D. Englund, G. W. Wornell, J. H. Shapiro, and F. N. C. Wong, *Photon-Efficient Quantum Key Distribution Using Time-Energy Entanglement with High-Dimensional Encoding*, New J. Phys. **17**, 022002 (2015).

[23] T. Sasaki, Y. Yamamoto, and M. Koashi, *Practical Quantum Key Distribution Protocol without Monitoring Signal Disturbance*, Nature (London) **509**, 475 (2014).

[24] H. Takesue, T. Sasaki, K. Tamaki, and M. Koashi, *Experimental Quantum Key Distribution without Monitoring Signal Disturbance*, Nat. Photonics **9**, 827 (2015).

[25] C. Schaeff, R. Polster, R. Lapkiewicz, R. Fickler, S. Ramelow, and A. Zeilinger, *Scalable Fiber Integrated Source for Higher-Dimensional Path-Entangled Photonic Qunits*, Opt. Express **20**, 16145 (2012).

[26] Z. Sun, A. Delteil, S. Faelt, and A. Imamoğlu, *Measurement of Spin Coherence Using Raman Scattering*, Phys. Rev. B **93**, 241302 (2016).

[27] R. Loudon, *The Quantum Theory of Light* (Oxford University Press, New York, 2000).

[28] D. Heiss, S. Schaeck, H. Huebl, M. Bichler, G. Abstreiter, J. J. Finley, D. V. Bulaev, and D. Loss, *Observation of Extremely Slow Hole Spin Relaxation in Self-Assembled Quantum Dots*, Phys. Rev. B **76**, 241306 (2007).

[29] K. De Greve, P. L. McMahon, D. Press, T. D. Ladd, D. Bisping, C. Schneider, M. Kamp, L. Worschech, S. Höfling, A. Forchel *et al.*, *Ultrafast Coherent Control and Suppressed Nuclear Feedback of a Single Quantum Dot Hole Qubit*, Nat. Phys. **7**, 872 (2011).

[30] S. G. Carter, S. E. Economou, A. Greilich, E. Barnes, T. Sweeney, A. S. Bracker, and D. Gammon, *Strong Hyperfine-Induced Modulation of an Optically Driven Hole Spin in an InAs Quantum Dot*, Phys. Rev. B **89**, 075316 (2014).

[31] D. Press, K. De Greve, P. L. McMahon, T. D. Ladd, B. Friess, C. Schneider, M. Kamp, S. Höfling, A. Forchel, and Y. Yamamoto, *Ultrafast Optical Spin Echo in a Single Quantum Dot*, Nat. Photonics **4**, 367 (2010).

[32] R. N. E. Malein, T. S. Santana, J. M. Zajac, A. C. Dada, E. M. Gauger, P. M. Petroff, J. Y. Lim, J. D. Song, and B. D. Gerardot, *Screening Nuclear Field Fluctuations in Quantum Dots for Indistinguishable Photon Generation*, Phys. Rev. Lett. **116**, 257401 (2016).

[33] X.-L. Wang, X.-D. Cai, Z.-E. Su, M.-C. Chen, D. Wu, L. Li, N.-L. Liu, C.-Y. Lu, and J.-W. Pan, *Quantum Teleportation of Multiple Degrees of Freedom of a Single Photon*, Nature (London) **518**, 516 (2015).

[34] https://doi.org/10.17863/CAM.22837.